Abnormal Slices Identification Technique using GLCM Features and Least Square Line Fitting Technique for MRI T2- FLAIR Brain Scans

T. Kalaiselvi

Assistant Professor
Department of Computer Science and Applications
Gandhigram Rural Institute Deemed University
Gandhigram, Tamilnadu
kalaiselvi.gri@gmail.com

S. Karthigai selvi

Research Scholar
Department of Computer Science and Applications
Gandhigram Rural Institute Deemed University
Gandhigram, Tamilnadu
karthigachandru@gmail.com

Abstract-**The proposed work is used to extract abnormal slices from a Magnetic resonance image (MRI) volume taken from an abnormal patient. This process is an essential part in brain image processing pipeline and is an initial work in any brain segmentation process. It drives the automatic diagnostic process to reach the target images directly and quickly. The proposed work is developed by using Gray level co occurrence matrix (GLCM) features and least square line fitting techniques. The neighborhood features related to hyper intense regions are targeted for constructing the GLCM. Then the mean value of each slice GLCM is processed to separate the abnormal range. Finally, the least square line fitting technique is used to fix the lower and the upper limits of abnormal range. 20 high grade tumor volumes and 10 low grade tumor volumes of T2-FLAIR sequences are taken from BRATS database. Among them some volumes are suspected by artifacts and some are in good quality for further processing. The 3D volumes are converted into 2D slices for our experiment. For 12 volumes, the proposed technique yields 97% accuracy. The experiments were also carried out on the other artifact affected volumes and the noisy volumes. It results that the proposed method detects the abnormal slices (image) with more accuracy in good quality volume and abnormal slices along with the noisy and artifact affected slices.**

Keywords- MRI, T2-FLAIR, GLCM, Abnormality, Partial differentiation, Least square, Artifacts, Noise.

I. INTRODUCTION

Magnetic resonance (MR) machines produce high spatial and contrast images. Thus they show rich distinction between soft tissues. They are widely used in medical diagnosis, especially in brain disease analysis [1]. MR machine produces images based on non harmful ionizing radiations [2-3]. Generally, it produces grayscale images. The gray level mainly depends on tissue parameters, Proton density (PD), spin lattice (T1) and spin spin (T2) relaxation times [4]. The PD is very homogeneous but may exhibit higher intensity for gray matter and white matter lesions, T1 and T2 are sensitive to local environment [5-6]. Recently, Fluid attenuated inversion recovery (T2-FLAIR) has replaced the PD images in white matter lesion detection [7-10]. It visualizes a wide range of lesions, particularly those in periventricular or sub cortical areas [11-12]. Thus, they allow easy detection of small and relatively low contrast lesions [10].

Generally, abnormal slice classification has been using supervised clustering, neural networks and knowledge based systems. Recently, the earlier clustering techniques are combined with knowledge based system [13] and artificial neural networks [14-15] and Fuzzy logics [16]. In the knowledge based systems [13][17-18] use Fuzzy C-means as initial step. Then they apply the tissue features [13] and symmetric measure [17] in T2 axial images. But the anatomical structure of the brain varies with different planes. On the basis of anatomical structure and tissue characteristics the labeling techniques are implemented to identify abnormality [19]. In the mean time, quantification of white matter hyper intensities is applied to detect lesion [20-23]. But each tissue has its own features and hence, feature based methods have been emerging recently. Fourteen textural features are suggested to classify the abnormality [24]. It can be extracted by Gray level co-occurrence matrix (GLCM). These features were implemented in neural network to obtain the abnormal slices [25] and segmentation [26]. Additionally, wavelet features are also used for abnormality detection and segmentation [27-28]. Statistical features along with K-Nearest neighbor (KNN) technique enrich the clustering techniques [29]. Its performance is overcome by Least square support vector machine (LS-SVM) [9][30] using GLCM, statistical [31] and textural features. While using the features the brain anatomical structures are avoided. In the above supervised classification, more number of images and its features are required to produce accurate results. Otherwise the supervised learning cannot produce more accurate results because the image quality depends on the machine type. Figure 1 shows gray level co occurrence values of normal and abnormal slices. It can vary regarding the magnetic strength. Hence, the proposed work chooses the image metric from the same volume.

Figure 1. Gray level co occurrence values of normal and abnormal slices

To minimize the feature extraction, a novel technique is developed by using GLCM and Least square line for detecting normal and abnormal slices from T2-FLAIR images that are obtained from the patients suspected with abnormality. In T2-FLAIR images the tumor are hyper intense and are affects continuous images. Hence the count of hyper intense is require for the abnormal slice detection. GLCM calculates how often a pixel with gray level value occurs either horizontally, vertically or diagonally to adjacent pixels. Least square and partial derivatives [32] are used to fit a line to separate the abnormal slices from all slices in a volume. The experiments were done with good quality abnormal volumes, artifact affected abnormal volume and noise added abnormal volume. The results of above cases were tabulated and discussed in this paper.

This paper is organized as follows. In section II, the proposed technique is discussed in detail. In section III, the performance analysis operators are given. The visual and quantitative results are presented in section IV. The proposed technique is concluded in Section V.

II. METHODOLOGY

The proposed technique consists of three stages to detect the abnormal slices from 2D T2-FLAIR images. The proposed technique adopts skull striped T2-FLAIR images and uses neighborhood features. These features are extracted by using GLCM technique. The GLCM values differ for normal and abnormal slices. Then the optimal values are obtained by applying least square straight line equation. The slices which are outside of the straight line are considered as abnormal slices.

Stage 1: Feature extraction using GLCM
Stage 2: Least square line fitting process
Stage 3: Identifying the abnormal slices

A. Features Extraction using GLCM

It is a two dimensional histogram. It considers the spatial relationship between pixels of different gray levels. It calculates the frequency of occurrence of a pixel with gray level value i occurs horizontally (0°), vertically (90°) and diagonally (45° and 135°) adjacent to a pixel with the value j. The proposed technique counts the neighboring pixels associated with intensity in $0°, 45°, 90°$ and $135°$.

$$C_{\Delta x \Delta y}(i,j) = \sum_{p=1}^{n} \sum_{q=1}^{m} \begin{cases} 1, & \text{if } I(p,q)=i \quad \text{and} \quad I(p+\Delta x, q+\Delta y)=j \\ 0, & \text{otherwise} \end{cases} \tag{1}$$

where Δx and Δy represent the offset value.

If the offset is (0, 1), it will consider the pair as its right side neighbor 0°. The offsets (-1,1), (0,-1) and (-1,-1) represent 45°, 90° and 135°. In (1), m and n are number of rows and columns of a matrix. p and q represent the pixel position. i and j represent the gray level values. It is shown in Figure 1. The first

column of Figure 1 consists of normal and abnormal images. The following columns contain the pixel counts of gray levels 2^6 and 2^7 with its neighbors in four angles 0, 45, 90 and 135 degree respectively. It ensures that the normal slice is having very less number of pixel counts in gray levels 2^6 and 2^7. These counts are high in abnormal slices due to abnormality in T2-FLAIR images having high intensity. Hence the proposed technique takes (i, j) as $(2^6, 2^7)$, $(2^7, 2^6)$ and $(2^7, 2^7)$. The mean of it, M_s is taken for each slice (s).

$$M_s = \frac{1}{4} \sum_{i=-1}^{0} \sum_{j=-1,1} \frac{1}{3} (C_{i,j}(2^6,2^7) + C_{i,j}(2^7,2^6) + C_{i,j}(2^7,2^7)) \qquad (2)$$

The M varies for normal and abnormal slices as shown in Figure 2. In this figure, the slice index value is taken in X axis and M value is taken in Y axis. The slices which have high M values are abnormal slices.

B. Least Square Line Fitting Process

Initially, the abnormal slices are observed by using mean of M_i. The slices which are having M above mean of M_i have abnormality. But the detection of starting and ending abnormal slices is very crucial. Hence, the slices below mean value $f(x_i,y_i)$ are taken to detect the beginning and ending abnormal slices.

$$f(x_i, y_i) = \{(x_i, y_i), \text{ iff } y_i < \text{Mean}(M) \qquad (3)$$

where x and y represent slice number and its M value.

The slices lesser than mean of M are shown in Figure 3. It shows that the M values are closer to form a straight line but their deviation is not linear. At this moment, Least square helps in fitting a straight line between non linear points [32].

With reference to slice index and M, (x_1, y_1), (x_2, y_2), … (x_m, y_m) are closer to straight line, fitting a straight line by

$$y = ax + b \qquad (4)$$

Consider the ordinates y_1, y_2, …, y_m. The line will be ax_1+b-y_1, ax_2+b-y_2, …

Then introduce a general deviation as follows,

$$\delta_i = ax_i + b - y_i \qquad (5)$$

which are the deviations of positive, negative or exactly zero. It depends on a and b. As a condition of optimality,
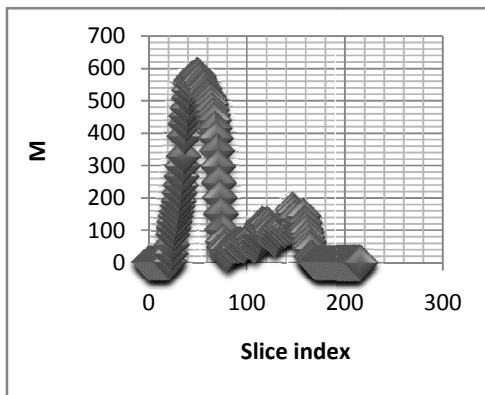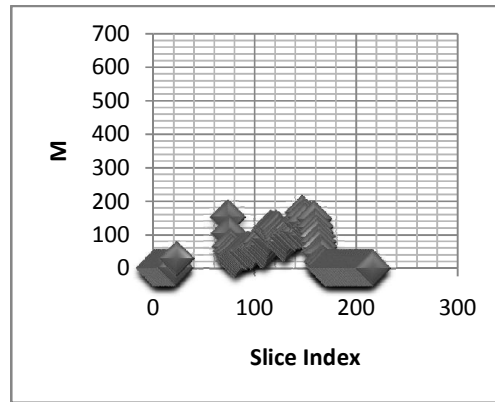

Figure 2. M of all slices

Figure 3. The slices below mean (M_i)

the sum of squares of deviation is minimized to determine a and b. Figure 2. depicts M of all slices. Figure 3. shows slices below mean.
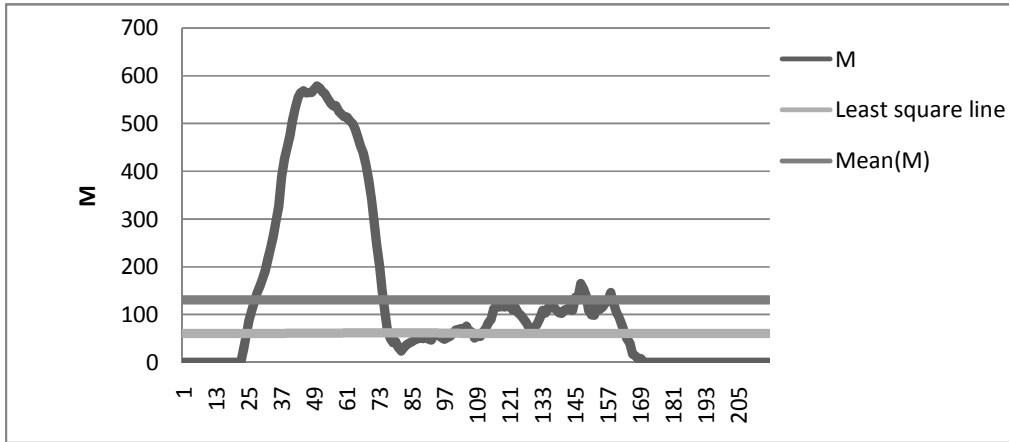
Figure 4. Least square line fitting

$$\sum_{i=1}^{m} \delta^2 \tag{6}$$

It is denoted by expression

$$s = \sum_{i=1}^{m} (ax_i + b - y_i)^2 \tag{7}$$

a and b are constants. Therefore, the derivatives depend on a and b which are zero.

$$\frac{\partial s}{\partial a} = 0, \frac{\partial s}{\partial b} = 0 \tag{8}$$

differentiating (7) depends on a is as follows

$$\frac{\partial s}{\partial a}(ax_i + b - y_i)^2 = 2(ax_i - b - y_i)x_i \tag{9}$$

taking summation in (9) is as follows

$$2\sum(ax_i + b - y_i)x_i = 0 \tag{10}$$

$$a\sum x_i^2 + b\sum x_i - \sum x_i y_i = 0 \tag{11}$$

differentiating (7) depends on b as follows

$$\frac{\partial s}{\partial b}(ax_i + b - y_i)^2 = 2(ax_i - b - y_i)1 \tag{12}$$

taking summation in (12) is follows

$$2\sum(ax_i + b - y_i) = 0 \tag{13}$$

$$a\sum x_i + bm - \sum y_i = 0 \qquad\qquad (14)$$

By simplifying (11) and (14), the a and b will be as follows

$$a = \frac{m\sum x_i y_i - \sum x_i y_i}{m\sum x_i^2 - (\sum x_i)^2} \qquad\qquad (15)$$

$$b = \frac{1}{m}\left(\sum y_i - a\sum x_i\right) \qquad\qquad (16)$$

Obtain a straight line by substituting a and b in (4)

C. Abnormal Slice Detection

A straight line obtained by Least square is used to cluster the slices. It is shown in Figure 4. The straight line derived by the Least square and partial differentiation is the mean value. It exactly divides the slices into two groups. For the exact detection of abnormal slices, the slice index which contains maximum M is obtained initially. Then a traversal is made from the slice to its left and right side of the slice until it reaches the line y obtained by (4). The traversed slices are taken as the abnormal slices.

D. Factors Affect Proposed Medthod

In real time clinical images noise and artifact such as intensity non uniformity (INU) are unavoidable one. Some unwanted signal equally distributed along an image is called noise. Generally, the noise in image acquisition process is Gaussian distribution. In MRI images, when the noise ratio is less than 3 is called Rician noises [33]. The unwanted signals affects the image unevenly is called artifacts. Generally, intensity non-uniformity (INU) artifact affects the slices. It is also known as intensity inhomogeneity artifact. This type of artifact arises due to non-uniform magnetic field produced by radio frequency coils and its environment [34]. In this type of images, intensity of the affected region shows high as tumor region in T2 FLAIR images. A sample INU affected MRI image is given in Figure. 5(a). In this image, the INU affected region is noted by a circle. A T2 FLAIR image with tumor is given in Figure. 5(b). The tumor region is marked by a circle. Both images are taken from a MRI volume. In both images, the regions denoted by circles are showing same intensity. It is an obstacle in automatic detection of abnormal slices. These slices can be justified by only medical experts. However, all type of imaging techniques produces numerous slices per patient. The slices may either contain normal tissues alone or may be with abnormal tissues. The intensity of abnormal tissue is mostly closer to the normal tissue [34]. Hence, rough segmentation of tissues affects the goal of abnormality extraction. Thus insists the abnormal slice classification as preprocessing technique in high level processing such as segmentation. In numerous slices, abnormal slice classification tired the radiologists. It clears the way and results in emergence of automatic slice classification techniques.
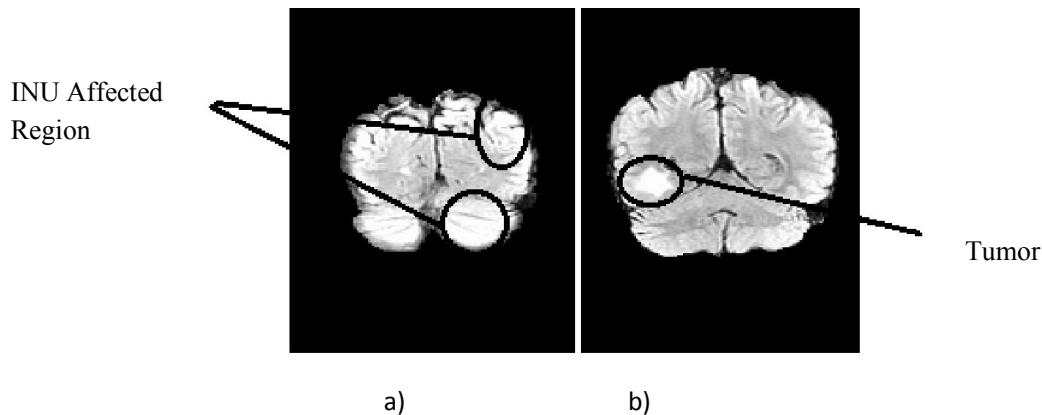

Figure 5. Sample MRI T2 FLAIR images. (a) INU affected image, (b) Tumor image

E. Evaluation Parameters

Sensitivity and specificity are the measures of the performance of a binary classification test. Sensitivity relates to the test's ability to identify abnormal slices correctly. Specificity relates to the test's ability to ignore

the normal slices in the result. Both attain 100%, it is for a maximum significance. Sensitivity, specificity and accuracy are used to evaluate the performance of the proposed technique.

$$\text{Sensitivity} = \frac{T_P}{T_P + F_N} \times 100 \tag{17}$$

$$\text{Specificit y} = \frac{T_P}{T_N + F_P} \times 100 \tag{18}$$

$$\text{Accuracy} = \frac{T_P + T_N}{T_P + F_N + T_N + F_P} \times 100 \tag{19}$$

True positive (TP) is the count of abnormal slices which are truly abnormal in nature. In the same way, true negative (TN) is the count of normal slices which are truly normal in nature. The count of abnormal slices as normal are called false negative (FN). Contradictory to FN, the counts of normal slices are classified as abnormal and are called false positive (FP).

False alarm (FA) and Missed alarm (MA) are used for evaluation. FA is an indication when the input scan without tumor is marked as abnormal during analysis. MA is an indication when an abnormal image is not marked during the analysis [35].

III. RESULTS AND DISCUSSION

For the experiments, T2-FLAIR images and the ground truth images were collected from BRATS website because this database contains numerous MRI images which were captured by various machines. This data base contains 3D image volumes. All 3D volumes were converted into 2D magnitude images with the help of 3DSlicer 4.3.0 and MRIcro software. Then the above algorithm has been coded using MATLAB 7.8 in Dual core 2 processor machine.Initially 20 tumor volumes of skull striped images are taken without any preprocessing techniques. In 20 volumes, 12 volumes (HG1, HG2, HG3, HG4, HG6, HG8, HG9, HG10, HG11, HG14, HG15, and HG27) are not affected by INU artifacts. The remaining volumes are suspected by INU which are showed as tumor intensity. Hence, in remaining volumes, the proposed technique detects the tumor slices along with INU affected slices.

TABLE I. ABNORMAL SLICE DETECTION RESULT

Volume ID (1)	Total slices (2)	Abnormal Slices		TP (5)	TN (6)	FP (7)	FN (8)	Sensitivity (9)	Specificity (10)	Accuracy (11)	Time (Sec.) (12)
		Manual (3)	Proposed technique (4)								
HG1	216	71-158	73-154	82	128	0	6	93.182	100	97.222	0.0469
HG2	216	24-75	24-77	52	162	2	0	100	98.78	99.074	0.0479
HG3	216	30-118	33-112	80	127	0	9	89.888	100	95.830	0.0519
HG4	216	74-136	76-136	61	153	0	2	96.825	100	99.074	0.0512
HG6	236	79-179	80-175	96	135	0	5	95.05	100	97.881	0.0631
HG8	176	35-144	41-149	104	61	5	6	94.545	92.421	93.75	0.0481
HG9	216	86-187	88-177	90	114	0	12	88.235	100	94.444	0.0497
HG10	216	38-73	39-80	35	173	7	1	97.222	96.111	96.296	0.0465
HG11	216	84-176	85-172	88	123	0	5	94.624	100	97.685	0.0477
HG14	216	107-175	104-170	64	144	3	5	92.754	97.959	96.296	0.049
HG15	216	88-175	86-172	85	126	2	3	96.591	98.438	97.685	0.051
HG27	230	57-173	56-175	117	110	3	0	100	97.345	98.696	0.0625
Average								**94.910**	**98.421**	**96.995**	**0.0513**

TABLE II. ABNORMAL SLICE DETECTION ALONG WITH INU SUSPECTED SLICES RESULT

Volume ID (1)	Total slices (2)	Abnormal slices		FA (5)	MA (6)	Volume ID (7)	Total slices (8)	Abnormal slices		FA (11)	MA (12)
		Manual (3)	Proposed (4)					Manual (9)	Proposed (10)		
HG5	216	22-105	25-151	46	3	LG2	236	77-179	81-173	0	10
HG7	216	56-169	37-155	33	0	LG4	236	60-137	32-148	40	0
HG12	216	106-143	43-163	83	0	LG6	216	104-159	30-165	80	0
HG13	216	64-95	36-164	98	0	LG8	236	127-167	76-173	57	0
HG22	230	77-158	41-144	36	14	LG11	230	81-138	42-173	74	0
HG24	240	71-148	43-148	28	0	LG12	216	108-165	43-164	65	1
HG25	230	92-168	38-90	54	78	LG13	220	70-146	31-179	72	0
HG26	220	51-189	31-130	20	59	LG14	230	77-128	42-183	90	0
LG1	196	54-102	35-130	46	0	LG15	230	149-194	37-120	84	42

The proposed technique detects tumor slices well in the 12 volumes. Two sample images are shown in Figure 6 (a) and Figure 6(b). Thus the quality (white matter and gray matter are distinguishable by vision) will be taken as standard quality in future for applying the proposed technique. The remaining images shown in Figure 6(c) and 6(d) cannot be processed by the proposed technique. Its results are illustrated in Table I. It consists of the 12 high grade tumor volumes, abnormal slice ranges and its T_P, T_N, F_P, F_N, sensitivity, specificity and accuracy. In this table, column 1 represents the volume number. Column 2 contains the slices in the coronal volume. Column3 specifies the range of abnormality mentioned by the medical experts. The range of abnormal slices detected by the proposed technique is given in column 4. The columns 5, 6, 7 and 8 show the counts of correctly detected abnormal slices (T_P), correctly detected normal slices (T_N), mistakenly identified as abnormal (F_P) and the abnormal slices are not detected as abnormal (F_N). The following columns 9, 10 and 11 show the sensitivity, specificity and accuracy for each volume respectively. The last column shows the time consumed by the proposed technique to detect the abnormal slices for the entire volume.

In Table I, column 12 shows that the proposed technique takes very less time to process an entire volume. With the reference of Table I, the proposed technique does not reveal normal slice as abnormal in the volumes HG1, HG3, HG4, HG6, HG9 and HG11. For the volumes, the proposed technique yields 100% of specificity. While processing HG2 and HG27, the proposed technique gives 100% sensitivity. Those represent the proposed technique does not leave the abnormal slices. The proposed technique attains 97% of accuracy in the process of 12 volumes. It ensures its performance.

Then the proposed technique is implemented in the 10 low grade tumor volumes. In these volumes, the proposed technique classifies the tumor and INU affected slices. The results are illustrated in Table II. In this table, the volume numbers are given in columns 1 and 7. Column 2 and 8 show the total number of slices in the respective volumes. The abnormal slice ranges selected by medical experts are given in column 3 and 9. The abnormal slices extracted by the proposed technique are given in column 4 and 10. Column 5 and 11 show the FA and MA. They represents that the proposed technique selects more slices beyond the tumor slices selected by experts. Our visual perception ensures that the slices are affected by artifacts. Hence, the proposed technique selects those slices along with tumor slices. HG25 and LG15 volumes are having more counts of INU affected

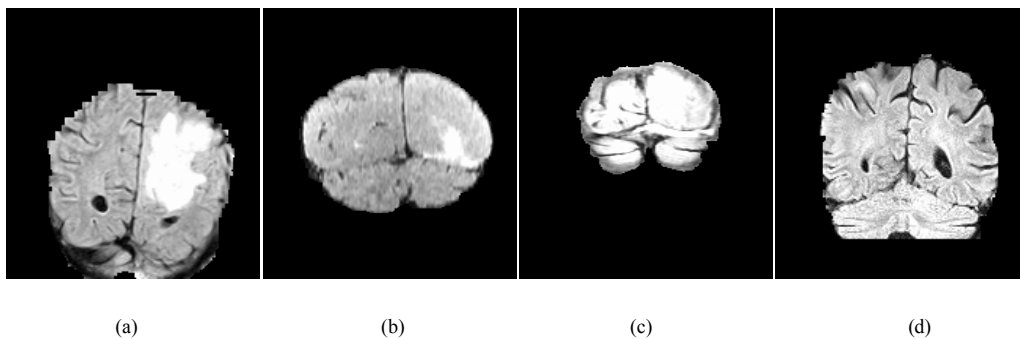|			
(a)	(b)	(c)	(d)

Figure 6. Image visual quality, (a). Sample image from HG2, (b). Sample image from HG27, (c). Sample image from LG15, (d). Sample image from HG25

slices. The INU affected slices are having maximum count of 2^6 and 2^7 gray level neighboring pixels than tumor suspected pixels. It is graphically represented in Figure 7. In this figure the slices in LG15 is represented in x axis and the mean of the GLCM of the intensity with 2^6 and 2^7 and given in y axis. Due to the INU artifact the graph has two peaks. The proposed method concentrates on a peak which is containing the maximum mean value. But in this volume the INU affected slices are having the maximum GLCM mean of 2^6 and 2^7 neighborhood count. Hence, the proposed method takes the peak which is produced by the INU affected slices. It is the limitation of the proposed method.
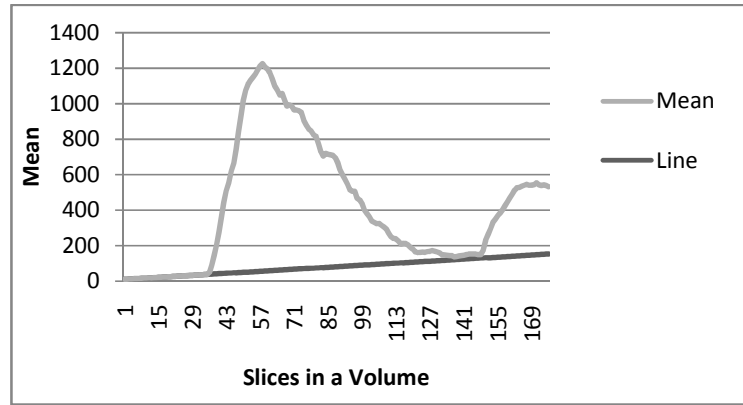

Figure 7. The GLCM mean of the intensity with 2^6 and 2^7 and Least square line

Finally, the experiment was done over noisy images. The noises are additive in nature such as Gaussian and Rician noise. Some volumes, in which the proposed method works well, are taken for the experiment. Initially, Gaussian noise in the variance 0.03, 0.05, 0.07 and 0.1 are applied on HG2, HG3, HG4, HG6 and HG8 volumes. Then the proposed technique was applied on those images. In the same way, 3, 5, 7 and 10 percentage of Rician noises were introduced in the HG2, HG3, HG4 and HG8 volumes. Then results were taken.

The noisy images and the graphical representation of the proposed method are given in Figure 8. In this figure, row 1 contains a clean image which is taken from HG4, a Gaussian noise (variance 0.1) applied image and a Rician noise (10%) applied image from left to right respectively. The results of proposed method on HG4 are graphically represented in the second row of Figure 8. Figure 8 (d)-(f) are the graphical representation of the proposed method results which contain the GLCM mean and the least square line observed by the method. Figure 8 (d) shows the result in clean image volume HG4, Figure 8 (e) and (f) show the result of proposed method derived from the Gaussian and Rician noise applied image volume (HG4) respectively. In Table III, the abnormal slice detection result in the noisy images and the time taken by the proposed method are given. In this table, the rows from two to six represent the abnormal slice detection result and the following rows contain the time consumption by the proposed technique to yield the result. The column 2 contains the volume ID. The column 3 contains the result of proposed technique before noise implementation. The columns 4 to 7 contains the abnormal slice detection result in various level (variance = 0.03, 0.05, 0.07 and 0.1) of Gaussian noises. The columns 8 to 11 gives the result of slice detection after the application of Rician noises in various percentages (3, 5, 7 and 10 percentages). Usually, the Gaussian noise is distributed evenly in all slices. Hence, the centre of the peak is not affected by this type of noise in good quality of images but the end slices are extended i.e. width of the peak increases. It is demonstrated in Figure 8 (d) and (e). According to Figure 8 (b) and (c), the Rician noise is not a white noise like Gaussian. Hence, Rician noise does not make tremendous changes in the result of these volumes compared to the noise free images. It is given in Figure 8 (a) and (f). The all results are illustrated in the Table III.
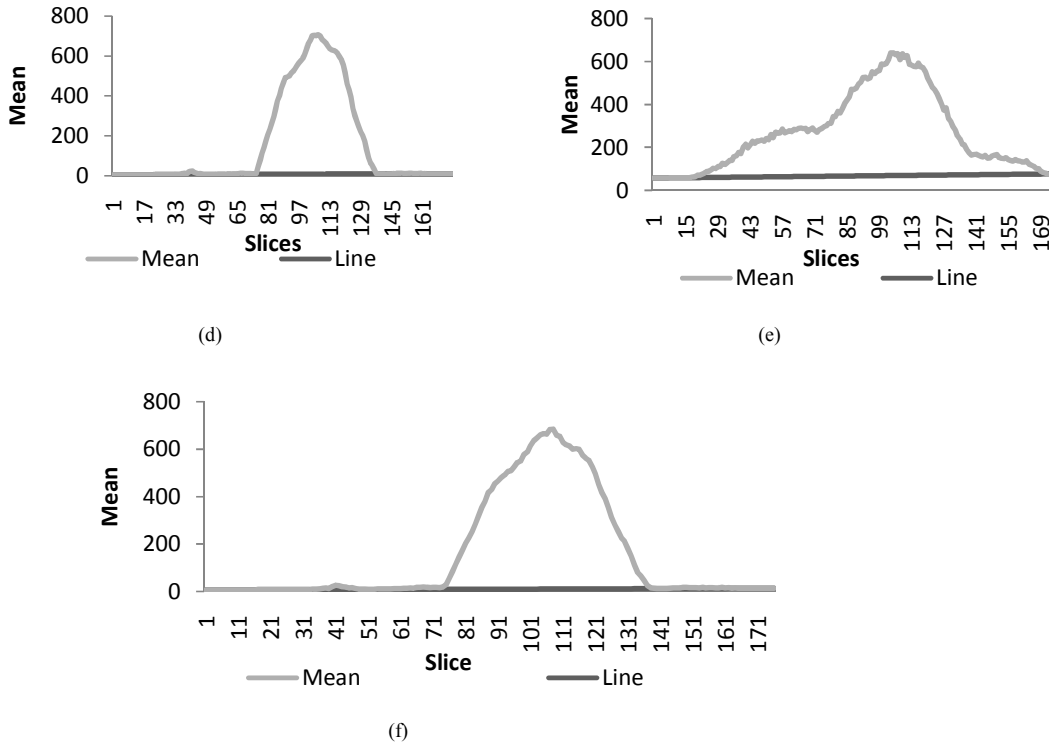

| (a) | (b) | (c) |

(d)

(e)

(f)
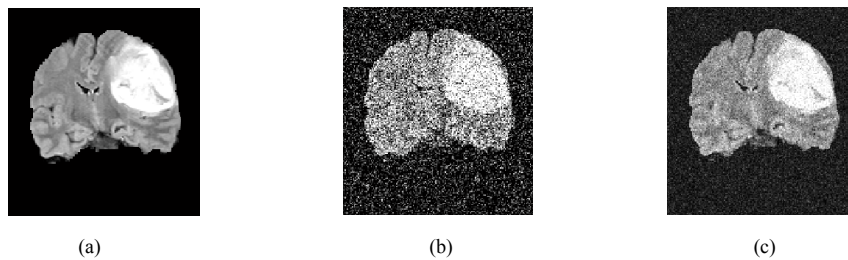
Figure 8. Noisy images and the least square line fitting technique result in noisy images. (a). Clean image, (b). Gaussian noise (σ=0.1) added image, (c). Rician noise (10%) added images. Result of proposed technique in (d). Clean image, (e). Gaussian noise (σ=0.1), (f). Rician noise (10%) added volume HG4

TABLE III. THE RESULT OF ABNORMAL SLICE DETECTION IN THE ADDITIVE NOISE SUSPECTED SLICES

(1)	Volume ID (2)	Clean volume (3)	Gaussian noise				Rician noise			
			$\sigma^2 = 0.03$ (4)	$\sigma^2 = 0.05$ (5)	$\sigma^2 = 0.07$ (6)	$\sigma^2 = 1.0$ (7)	3% (8)	5% (9)	7% (10)	10% (11)
Abnormal slice detected by the proposed method	HG2	24-77	24-165	24-165	24-165	24-165	24-79	25-164	25-163	25-164
	HG3	33-112	34-149	33-149	33-169	33-169	33-117	33-116	33-116	33-117
	HG4	76-136	38-141	38-164	34-165	25-173	75-136	75-137	75-137	65-137
	HG6	80-175	76-178	75-179	75-179	75-179	80-175	80-175	80-175	80-176
	HG8	41-149	39-154	40-155	40-156	41-156	40-142	40-141	40-141	39-152
Time	HG2	0.047	0.045	0.048	0.048	0.052	0.045	0.049	0.045	0.050
	HG3	0.052	0.051	0.053	0.057	0.054	0.058	0.051	0.048	0.052
	HG4	0.051	0.045	0.045	0.046	0.048	0.050	0.047	0.052	0.046
	HG6	0.063	0.055	0.059	0.066	0.064	0.05	0.061	0.055	0.057
	HG8	0.051	0.050	0.048	0.049	0.044	0.050	0.048	0.050	0.048

According to the Tables I and III, Gaussian noise only affect the range of abnormal slices compared to the Rician noise. In HG2 volume, the Gaussian and Rician noises affected the result of abnormal slice selection. In the volume HG3 Rician noise did not affect the result but Gaussian noise affect the range of slice selection. In

other volumes, HG4, HG6 and HG8 both noises were not affect the result tremendously. Generally, in noisy image volumes the proposed method selects the abnormal slices along with some normal slices. Even though, the proposed technique takes very lesser time on the noisy images also. Through this experiment carried out on various machine images, it is concluded that the proposed technique helps in extracting the abnormal (tumor and INU artifact) affected slices. Thus it helps to preprocess the resulted slices only before starting the high level processing. It offers lesser time conception in segmentation.The proposed technique does not concentrate on geometrical features. Hence, it can process all orientation (coronal, sagital and axial) T2-FLAIR images.

IV. CONCLUSION

In this paper, a novel classification technique is proposed to detect abnormal slices from 2D T2-FLAIR sequence. The abnormality may be tumor or artifacts. It uses neighborhood features like GLCM, as well as least square line generation with partial differentiation. With lesser effort and lesser time, it can yield good sensitivity and accuracy. To ensure this, 20 volumes of T2-FLAIR skull stripped sequence images are used for testing without adopt preprocessing like denoising and artifact removal. Out of them, it yields more than 98% accuracy for 2 volumes, 97% accuracy for 5 volumes and above 94% accuracy for 5 volumes are obtained. In INU affected volumes, the proposed technique detects the noise and INU affected slices along with tumor slices. It takes very lesser time (0.05 sec.) to detect the slices in a volume. It can perform in all orientation of T2-FLAIR images. It is very sensitive in terms of intensity. Hence, it cannot exactly detect abnormal slices in artifact affected images. In future, artifact removal process will employ in the output of the proposed technique. Further its performance will be compared with existing methods.

REFERENCES

[1] K. Somasundaram, S. Vijayalakshmi, T. Kalaiselvi, "Segmentation of brain portion from MRI of head scans using K-Means cluster", International Journal of Computational Intelligence and Informatics, vol. 1,no. 1, pp. 75-79, 2011.

[2] J. G. Webster, "Medical instrumentation application and design", John Wiley and Sons Inc. New York, pp. 551-555, 1998.

[3] E. Mark Haacke, Robert W. Brown, Michael R. Thompson, Ramesh Venkatesan, "Magnnetic resonance imaging physical principles and sequence design", Wieley –Liss, New York, 1999.

[4] T. Kalaiselvi, "Brain portion extraction and brain abnormality detection from Magnetic resonance imaging of human head scans", Pallavi Publications India Pvt. Limited, India, 2011.

[5] N. B. Karayiannis, Pin-I pai, "Segmentation of Magnetic resonance images using Fuzzy algorithms for learning vector quantization", IEEE transactions on Medical imaging, vol.18(2), pp.172-180, 1999.

[6] C. A. Cocosco, A. P. Zijdenbos, A. C. Evan, " Fully anatomic and robust brain MRI tissue classification method", Medical image analysis, vol. 7, pp. 513-527,2003.

[7] J. R. Heselink, "Basic principles of MRI imaging", Research report, Department of Radiology, University of California, 1997.

[8] Yi Zhong, David Utriainen, Ying Wang, Yan Kang, E. Mark Haacke, " Automated white matter hyperintensity detection in multiple sclerosis using 3D T2 T2-FLAIR", International Journal of Biomedical Imaging System Applications, vol. 2014, 2014.

[9] H. Selvaraj, S. Thamarai selvi, D. Selvathi, L. Gewali, "Brain MRI slice classification using Least square support vector machine", Interrnational Journal of Intelligent Computing in Medical Sciences and Image Processing, vol. 1(1), pp. 21-33, 2007.

[10] Fumihito Yoshii, Hitoshi Tomiyasu, yukito Shinohara, "Fluid attenuation inversion recovery (T2-FLAIR) images of dentatorubropallidoluysian atrophy", Journal of Neurology, Neurosurgery and Psychiatry, vol. 65, pp.369-399, 1998.

[11] J. V. Hajnal, B. De Coene, P. D. Lewis, C. J. Baudouin, F. M. Cowan, J. M. Pennock, I. R. Young, G. M. Bydder, "High signal regions in normal white matter shown by heavily T2-weighted CSF nulled IR sequence", Journal of Computer Assited Tomography, vol. 16, pp. 506-513, 1992.

[12] B. De Coene, J. V. Hajnal, P. Gatehouse, "MR of the brain using fluid attenuation inversion recovery (T2-FLAIR) pulse sequence", AJNR American Journal of Neuroradialogy, vol. 13, pp. 1555-1564, 1992.

[13] Chunlin Li, B. Dmitry, Goldgof, Lawrence O. Hall ,"Knowledge based classification and tissue labeling of MR images of human brain", IEEE transaction on medical imaging, vol. 12, pp. 740-750,1993.

[14] K. D. Kharatl, P. P. Kulkarni, M. B. Nagori, "Brain tumor classification using neural network based methods", Interrnational Journal of Computer Science and Informatics, vol. 1, pp. 85-90, 2012.

[15] Ahlam Fadhil Mahmod, Ameem Mohammed Abd Alsalam, "Automatic Brain MRI slice classification using Hybrid Technique", AI – Rafidain Engineering, vol. 22, 2014.

[16] S. Murugavalli, V. Rajamani, "An improved implementation of brain tumor detection using segmentation based on neuro fuzzy technique", Journal of computer science, vol. 3, pp. 841-846, 2007.

[17] K. Somasundaram, T. Kalaiselvi, "Fully automatic method to identify abnormal MRI head scan using Fuzzy segmentation and Fuzzy symmentric measure", International Journal of Graphics Vision and Image Processing, vol. 10, pp. 1-9, 2010.

[18] M. C. Clark, L. O. Hall, D. B. Goldgof, L. P. Clarke, R. P. Velthuizen, M. S. Silbiger, "MRI segmentation using fuzzy clustering techniques", IEEE Engineering in Medicine and Biology, pp. 730-742, 1994.

[19] C. Li, D. Goldgof, L. Hall, "Automatic segmentation and tissue labeling of MR brain images", IEEE Transaction of Medical Imaging, vol.12, pp.740-750, 1993.

[20] Mitsuhiro Yoshita, Evan Fletcher, Charles Decarli, "Current concepts of analysis of cerebral white matter hyperintensities on Magnetic resonance imaging", Top Magnetic Resonance Imaging, vol. 16, pp.399-407, 2005.

[21] D. Mortazavi, A. Z. Kouzani, Soltanian – Zadeh, "Segmentation of multiple sclerosis lesions in MR images a review", Neuro radiology, vol. 54, pp.299-320, 2012.

[22] P. Schmidt, C. Gaser, M. Arsic, "An automated tool for detection of T2-FLAIR- hyperintense white matter lesions in multiple sclerosis lesions in MR images", Neuroimage, vol.59, pp.3774-3783, 2012.

[23] T. Magome, H. Arimura, S. Kakeda, "Automated segmentations method of white matter and gray matter regions with multiple sclerosis lesions in MR images", Radiological physics and Technology, vol. 4, pp. 61-72, 2012.

[24] R. M. Haarlick, K. Shanmugan, I. Dinstein, "Textural features for image classification", IEEE Transaction on systems man and cybernetics, vol. 3, pp. 610-621, 1973.

[25] Nitish zulpe, Vrushen pawar, "GLCM Textural features for brain tumor classification", International Journal of Computer Science Issues, vol. 9, pp.354-359, 2012.

[26] Q. UI-Ain, G. Latof, S. B. Kazmi, M. A. Jaffar, A. M. Mirza, "Classification and segmentation of brain tumor using texture analysis", AIKED '10 Proceedings of the 9th WSEAS International conference on Artifitial Intelligence, Knowledge engineering and data bases, Cambridge, U.K, 2011.

[27] K. M. Iftekharuddin, S. Ahmed, J. Hossen, "Multiresolution texture models for brain tumor segmentation in MR",. 33rd Annual international conference of the IEEE EMBS, Boston, Massachusetts, USA, pp. 6985-6988, 2011.

[28] M. S. Sumesh, C. Gopakumar, Rejirajan Varghese, Abraham Varghese, "Level based normal abnormal classification of MRI brain images", International Journal of Computer Engineering and Technology, vol. 4,no. 2, pp.403-409, 2013.

[29] R. J. Ramteke, Y. Khachane Monali, "Automatic medical image classification and abnormality detection using K – Nearest neighbor", International Journal of Advanced Computer Research, vol. 2, pp.190-196, 2012.

[30] J. A. K. Suykens, T. Vandewalle, "Least square support vector machines", Neural Processing Letter, vol. 9, pp.293-300, 1999.

[31] T. Hastie, R. Tibshirani, J. Friedman,"The elements of statistical learning", Springer Verlag, 2003.

[32] Edward Batschelet, "Introduction to mathematics for life scientists", 3rd Edition, Springer Verlag, 2003.

[33] T. Kalaiselvi, S. Karthigai selvi, "A novel Wavelet thresholding technique to denoise magnetic resonance images", National conference on Recent Trends in Intelligent System, University of Madras, India, March. 2015.

[34] Chunming Li, Chick-Yen Kao, John C. Gore, Zhaokua Ding, "Implicit active contours driven by local binary fitting energy", IEEE conference CVPR'07, Computer Vision and Pattern Recognition, pp. 1-7, 2007.

[35] T. Kalaiselvi, K. Somasundaram, M. Rajeswari, "Fast brain abnormality detection method for magnetic resonance images (MRI) of human head scans using K-Means clustering technique", Proc. 4th Inter. Conf. on signal and image processing, Lecture notes in Electrical engineering, pp. 225-234. 2013.